Measurement of prompt neutron spectra from the ^{239}Pu(n,f) fission reaction for incident neutron energies from 1 to 200 MeV

A. Chatillon,* G. Bélier, T. Granier, B. Laurent, B. Morillon, and J. Taieb
CEA, DAM, DIF, F-91297 Arpajon, France

R. C. Haight, M. Devlin, R. O. Nelson, S. Noda, and J. M. O'Donnell
LANSCE, Los Alamos National Laboratory, MS H855, Los Alamos, New Mexico 87545, USA
(Received 28 October 2013; published 15 January 2014)

Prompt fission neutron spectra in the neutron-induced fission of ^{239}Pu have been measured for incident neutron energies from 1 to 200 MeV at the Los Alamos Neutron Science Center. Mean energies deduced from the prompt fission neutron spectra (PFNS) lead to the observation of the opening of the second chance fission at 7 MeV and to indications for the openings of fission channels of third and fourth chances. Moreover, the general trend of the measured PFNS is well reproduced by the different models. The comparison between data and models presents, however, two discrepancies. First, the prompt neutron mean energy seems constant for neutron energy, at least up to 7 MeV, whereas in the theoretical calculations it is continuously increasing. Second, data disagree with models on the shape of the high energy part of the PFNS, where our data suggest a softer spectrum than the predictions.

DOI: 10.1103/PhysRevC.89.014611 PACS number(s): 25.85.Ec

I. INTRODUCTION

Prompt fission neutron spectra (PFNS) are not only an important parameter for nuclear data evaluation for applications, but can also be relevant for a more fundamental understanding of the fission process. Experimentally the current knowledge of PFNS is sustained by few data far less precise than the ones of other key fission observables such as fission cross sections and prompt neutron multiplicities. And from the theory point of view, microscopic theoretical models are not yet able to predict precisely the fission observables. Hence, evaluated PFNS used in the libraries are obtained from phenomenological models. Concerning the data evaluation, PFNS need to be accurately known especially for nuclear criticality predictions. As summarized in [1], PFNS as currently evaluated in the different libraries may have systematic errors leading to an evaluation of spectra being too hard. In [2], disagreements between differential and integral measurements and their impact on the multiplication factor K_{eff} are discussed. A new shape for PFNS is proposed with more neutrons in the low-energy part and fewer in the high-energy part. Moreover, new Monte Carlo Hauser Feshbach calculations [3,4] seem to agree with this hypothesis. With the current experimental measurements of the PFNS, whose shape is still poorly known, it is not yet possible to test the different approaches. For more fundamental aspects, a recent model [5–7] describes the fission process with a constant temperature level density, each nascent fragment having its specific temperature. This model makes a new assumption for the partition of the intrinsic excitation energy between the two fission fragments in contact: Most of the intrinsic excitation energy of the fragment with the higher temperature is transferred to the fragment with the lower temperature. Under this hypothesis, called the energy sorting hypothesis, all the fission observables can be deduced. Because the mean energy can be extracted from the PFNS and is an indirect measurement of the nuclear temperature, PFNS can also be a sensitive test for this new model. Finally, this discussion on the excitation energy sharing is also of major importance for the data evaluation, because it is one of the ingredients which determine the high-energy component of PFNS as stressed in [3], where this approach is compared to the Madland-Nix approach [8].

To measure PFNS with consistent error uncertainties over a broad incident neutron energy range (from 1 to 200 MeV), an experimental campaign was started in 2002 in the framework of a collaboration between CEA-DAM and the Los Alamos National Laboratory. PFNS in ^{235,238}U(n,f) and ^{237}Np(n,f) have already been successfully studied [9–11]. A first experiment on ^{239}Pu was done in 2007 [12], but suffered from a high background level. This paper reports on results obtained during a second measurement of PFNS in ^{239}Pu(n,f) performed in 2008.

In Secs. II and III the experimental conditions and data analysis are detailed. Then the experimental PFNS and mean energies are shown and compared to evaluation in Sec. IV, before being discussed in Sec. V.

II. EXPERIMENTAL SETUP

A. Production of the neutron beams at the WNR facility

The WNR facility delivers white and pulsed neutron beams [13] with an energy spread from below 1 to several hundreds of MeV with a maximum intensity around 2 MeV.

Neutrons are produced by spallation reactions induced by an 800-MeV pulsed proton beam impinging on a tungsten target. Neutrons are collimated on several flight paths (Fig. 1). The experiment was installed on the 30° right flight path and located 22.7 m away from the spallation target. The beam spot size was 2.8 cm in diameter at the ^{239}Pu target position.

*audrey.chatillon@cea.fr

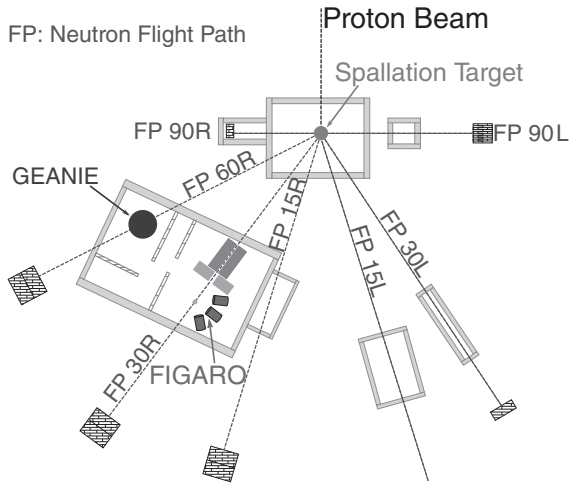

FIG. 1. Schematic view of the WNR facility at the LANSCE. The FIGARO setup is located on the 30° right flight path.

Because the beam is pulsed, the slowest neutrons from one pulse reach the fission target at the same time as the fastest neutrons from the following pulse. This wrap-around effect was reduced by inserting 2.54 cm polyethylene into the beam line to remove the slowest neutrons. An additional 1.27 cm of lead attenuated γ rays from the source. Data were taken during two weeks (effective time) with a rate of about 25 fissions per second.

B. Detection system

The target used was a multilayer fission chamber containing a total amount of 100 mg of ^{239}Pu distributed over 20 layers. Each layer consisted of ^{239}Pu material deposited on a thin metal backing. The body of the chamber was made of aluminum. The signal of the chamber, produced when a fission occurred, was used to trigger the data acquisition system.

The neutron detector array FIGARO [14] was used to measure the prompt fission neutrons in coincidence with the fission chamber signals (Fig. 2). FIGARO consists of 20 EJ301 organic liquid scintillators (NE213 equivalent) surrounding the fission chamber at a distance of about 1 m and on several

FIG. 2. (Color online) Experimental setup is as follows: FIGARO neutron detectors surrounding the fission chamber are located on seven different detection angles (45°, 60°, 75°, 90°, 105°, 112°, and 135°) with respect to the beam direction.

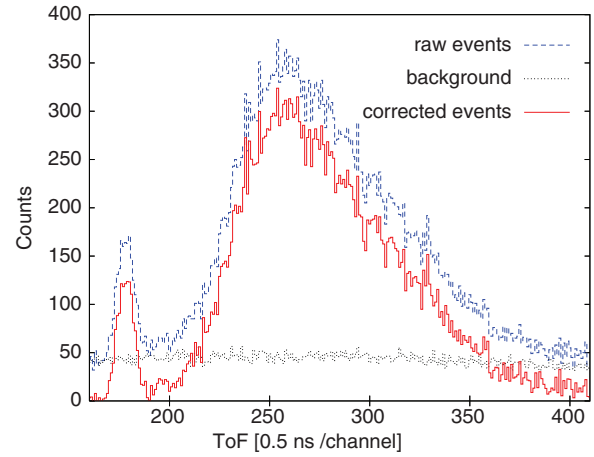

FIG. 3. (Color online) Example of the scattered neutron component subtraction on one neutron time-of-flight spectrum for all incident neutron energies and after neutron–γ-ray discrimination: (dashed line) raw time-of-flight spectrum, (dotted line) background contribution from scattered neutrons, (solid line) corrected time-of-flight spectrum. The peak on the left side corresponds to undiscriminated prompt fission γ rays, whereas the broad peak is from the selected prompt fission neutrons.

different detection angles (from 45° to 135° with respect to the beam direction). Organic scintillators are sensitive to neutrons and γ rays. Moreover, EJ301 exhibits good pulse shape discrimination properties. Therefore, neutrons and γ rays can be discriminated via a pulse shape analysis based on the charge integration of the short- and long-time components of the pulses. Finally, the electronic threshold was set to 300-keV neutron energy for all detectors.

III. DATA ANALYSIS

The experiment was based on the double time-of-flight method. For each triggered event, two times of flight were measured in coincidence. The first measurement was dedicated to the time of flight of the incoming neutron from the spallation target to the fission chamber and from this value, the energy of the incident neutron was calculated. The second measurement, coupled to the neutron–γ-ray discrimination, allowed us to obtain the time of flight of the prompt fission neutron from the target to the scintillator. The resolution of this measurement was 3.5 ns full width at half maximum (FWHM). The energy of the prompt fission neutrons was calculated from this time of flight.

Two corrections were applied to the prompt fission neutron time of flight. The first one (see Fig. 3) concerned a non-negligible background component mainly from the incident neutrons scattering off the fission chamber structure (windows and backings). These scattered neutrons were not correlated with fission and created background in the neutron detectors through random coincidences. To subtract offline this background component, a second trigger, a pulser at 100 Hz, was set to monitor precisely the contribution of scattered neutrons, as a function of the beam energy. During this experiment, the signal-to-background ratio was about 4:1, which is a significant improvement compared to the previous experiment [12] where we had a signal to background ratio

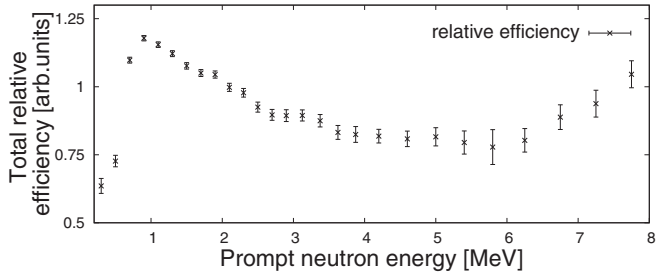

FIG. 4. Measured relative efficiency for the total FIGARO detection system.

equal to 1 because of the fission chamber having a thicker body made of stainless steel. Therefore, in the 2008 experiment the scattering of incoming neutrons and fission neutrons was reduced. Each raw time-of-flight spectrum (before neutron–γ-ray discrimination) showed a small and sharp peak, located 16 ns behind the fission γ peak. This was understood as prompt fission γ shifted in time because of an electronics problem during the experiment on the fission chamber signal. The peak area was used to determine the contribution of bad triggering events, which was evaluated to correspond to 10% of the total number of events. The second correction subtracted this shifted distribution.

For each detector, time-of-flight spectra were measured for many bins of incoming neutron energy. Those spectra were converted into energy spectra. The efficiency of each neutron detector was measured as a function of the prompt fission neutron energy. For this purpose, dedicated runs with beam off were performed with a ^{252}Cf source located on top of the fission chamber. During these runs, the acquisition was triggered by the γ ray emitted during the ^{252}Cf(sf) decay and detected by a $LaBr_3$ detector located at 25 cm from the source. Each PFNS measured by each FIGARO detector was then compared with the recommended evaluation by Mannhart [15].

Figure 4 and Table I present the measured relative efficiency for all the FIGARO detectors. First, the efficiency is increasing

TABLE I. Efficiency correction parameters for the prompt energy bins.

Neutron energy (MeV)	Relative efficiency (a.u.)	Neutron energy (MeV)	Relative efficiency (a.u.)
0.2–0.4	0.6355 ± 0.0275	3.0–3.25	0.8945 ± 0.0205
0.4–0.6	0.7268 ± 0.0211	3.25–3.5	0.8750 ± 0.0228
0.6–0.8	1.0976 ± 0.0109	3.5–3.75	0.8321 ± 0.0255
0.8–1.0	1.1783 ± 0.0098	3.75–4.0	0.8246 ± 0.0292
1.0–1.2	1.1546 ± 0.0102	4.0–4.4	0.8184 ± 0.0252
1.2–1.4	1.1217 ± 0.0110	4.4–4.8	0.8083 ± 0.0285
1.4–1.6	1.0767 ± 0.0120	4.8–5.2	0.8159 ± 0.0336
1.6–1.8	1.0504 ± 0.0128	5.2–5.6	0.7951 ± 0.0426
1.8–2.0	1.0447 ± 0.0132	5.6–6.0	0.7783 ± 0.0640
2.0–2.2	0.9978 ± 0.0151	6.0–6.5	0.8030 ± 0.0433
2.2–2.4	0.9778 ± 0.0159	6.5–7.0	0.8882 ± 0.0454
2.4–2.6	0.9251 ± 0.0185	7.0–7.5	0.9378 ± 0.0493
2.6–2.8	0.8966 ± 0.0200	7.5–8.0	1.0458 ± 0.0496
2.8–3.0	0.8938 ± 0.0216		

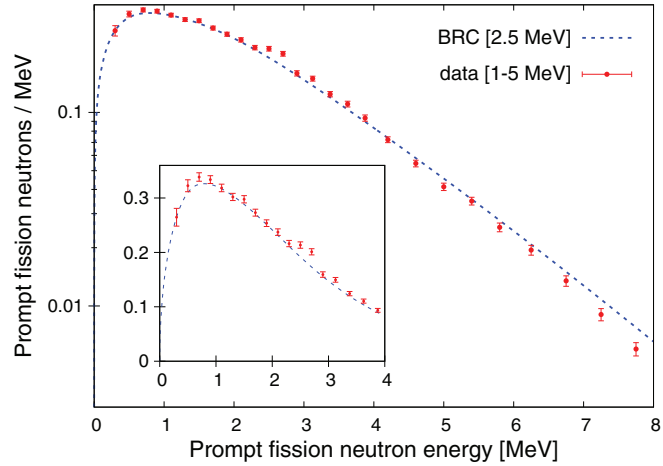

FIG. 5. (Color online) (Solid circles) PFNS obtained in coincidence with incident neutrons from 1 to 5 MeV. (Dashed line) BRC evaluation of PFNS for an incident neutron of 2.5 MeV. The inset shows the lower part of the same spectrum but on a linear scale.

up to 900 keV and then is slowly decreasing up to 5 MeV. Above this energy, the curve tends to be flat and then goes slightly up. However, at this point error bars are large because of the lack of statistics. Furthermore, a recent study [16] shows that such a method might overestimate the efficiency response at higher energy because of the emission of delayed or isomeric γ rays in ^{252}Cf(sf). Interpretation on the high-energy part of PFNS should be dealt with carefully.

IV. RESULTS

A. PFNS

The final spectrum for a given incoming neutron energy range was then obtained by combining 15 normalized spectra. Data from five detectors were rejected (two at 45°, and the others at 60°, 75°, and 105°) because they did not show the proper neutron-γ-ray discrimination. We normalized all experimental PFNS to the evaluated spectrum at 1.5 MeV, obtained by Bruyères le Châtel (BRC) calculations, based on the Los Alamos model [8], following the prescription explained in [17] and with the prefission neutron spectra arising from Hauser-Feshbach calculations. Normalization factors for each incident neutron energy bin are obtained to have the same integral in both experimental and evaluated spectra, calculated from 1 to 7 MeV. All results are presented with the absolute statistical error bars, propagated through the data analysis to take into account all the corrections detailed previously, from the background subtraction to the efficiency correction. Figure 5 shows the measured spectrum of the prompt fission neutrons detected in coincidence with incident neutrons from 1 to 5 MeV (with a mean energy about 2.7 MeV). In the same figure, the evaluated spectrum with BRC is also reported (dashed line) for an incident neutron energy of 2.5 MeV, comparable to the mean incident neutron energy. The agreement between experimental points and the BRC calculation is fair except around 2.5 MeV, where the data present a structure that is not understood. It might correspond to an experimental bias. The problem cannot originate from the neutron detector, otherwise the effect would

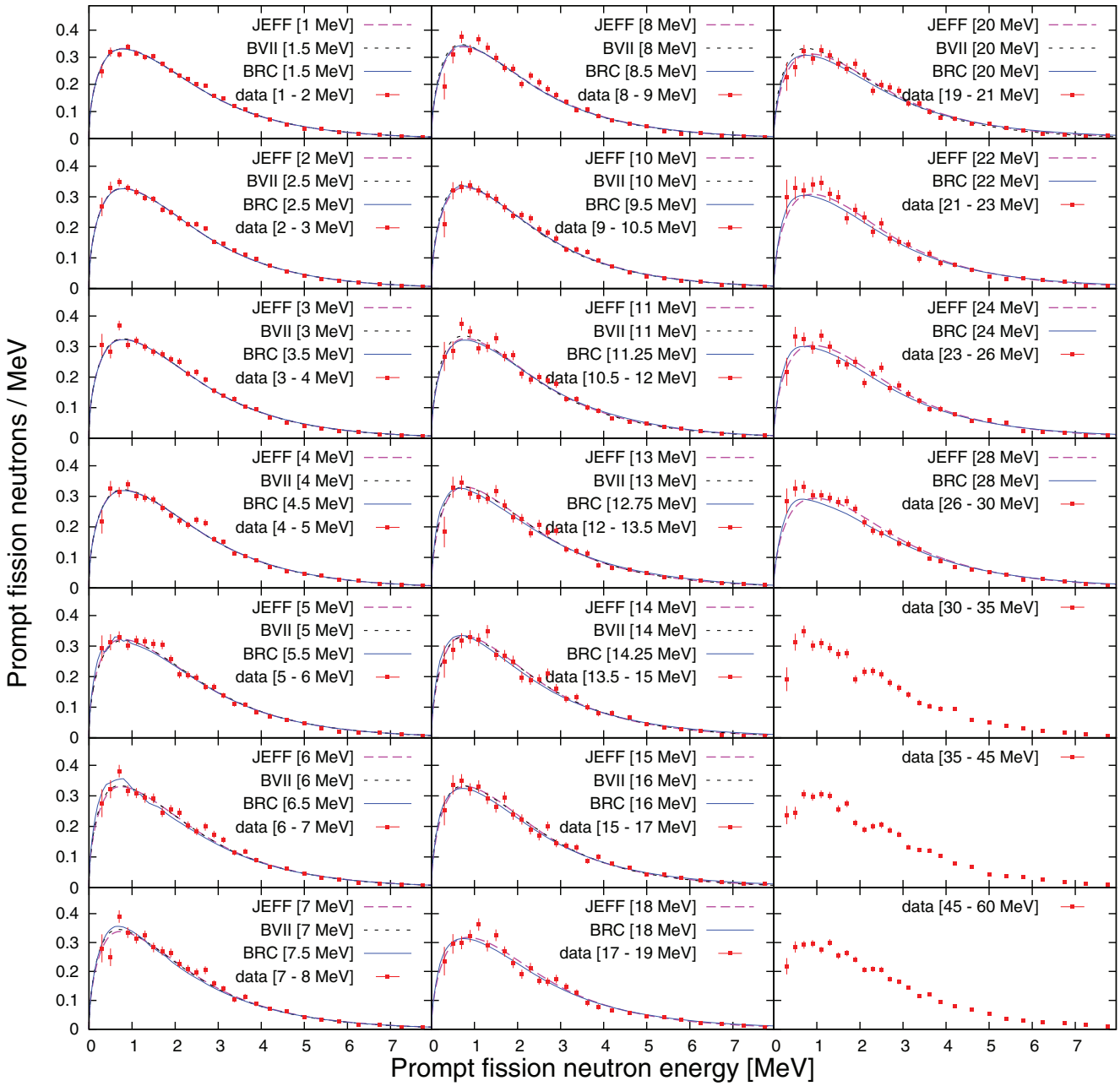

FIG. 6. (Color online) PFNS for several beam energies (indicated inside the square brackets). Experimental data (points) are compared to BRC calculation (solid line), JEFF 3.1 (dashed line), and ENDF/BVII.1 (dotted line) evaluations.

have been seen also in the efficiency calibration and therefore would divide out in the analysis. Moreover, at high energy the experimental points are below the evaluation. However, it is difficult to conclude because the efficiency correction might slightly bias the data, as previously explained (see Sec. III). We note that the efficiency curves differ from that of Ref. [12], and this difference is partly responsible for the differences of the shape of the deduced PFNS.

Figure 6 presents spectra for several incident neutron energy bins. The width of these bins is a compromise between statistics and a fine description of the evolution of the PFNS with incident neutron energy. In this figure the experimental data are compared to BRC, JEFF 3.1, and ENDF/BVII.1 evaluated spectra. The three calculations have the same trend up to the second chance fission. Above this value there are some slight discrepancies at low energy. However, our data are not precise enough and do not cover the very low-energy range to discriminate between the different approaches. To be independent of the efficiency correction, we can also study the evolution of the shape of the PFNS with increasing neutron beam energy by plotting the ratio of each spectrum versus the spectrum obtained for 1–2 MeV incoming neutrons. In Fig. 7 these ratios are represented and compared to BRC, JEFF 3.1, and ENDF/BVII.1 evaluations. Above 5 MeV, the data suffer from a lack of statistics. But still, the agreement between experiment and models is good within the error bars.

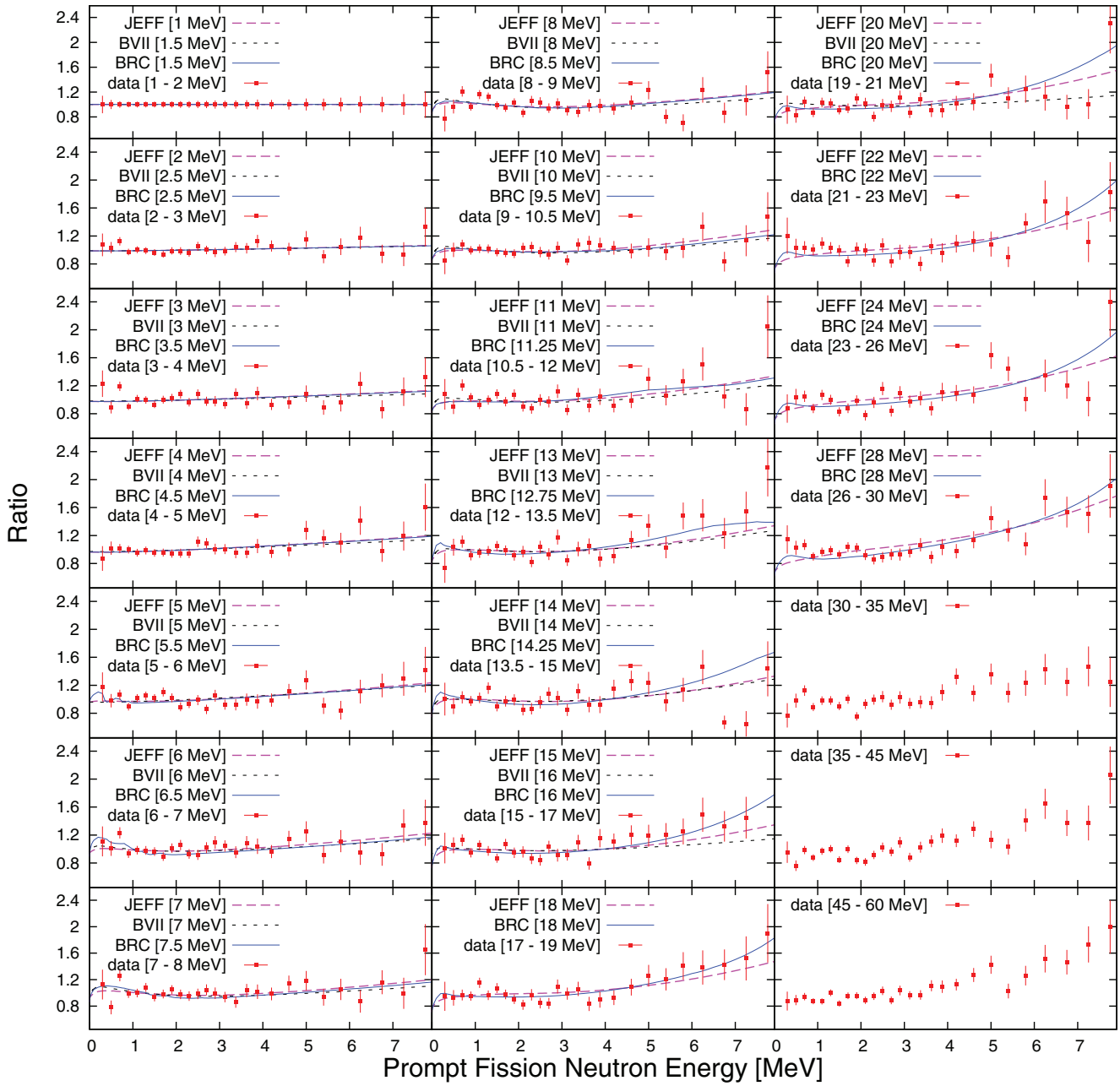

FIG. 7. (Color online) First spectrum (top, left), measured and evaluated PFNS for a neutron beam energy indicated inside square brackets. All other spectra, ratio of the PFNS obtained for several beam energies (indicated inside the square brackets) over the first PFNS (top left) obtained for a beam energy around 1.5 MeV. Experimental data (points) are compared to BRC calculation (solid line), JEFF 3.1 (dashed line), and ENDF/BVII.1 (dotted line) evaluations.

It confirms a progressive hardening of the spectral shape as the incident neutron energy increases.

B. Mean energies

For each spectrum, we calculated the prompt fission neutron mean energy from 400 keV to 7 MeV. Above 7 MeV, the statistics are poor. Below 400 keV, the limit of the pulse shape discrimination is reached and the efficiency of the EJ301 decreases strongly.

In Fig. 8, the experimental results, measured with uncertainties better than 2%, are compared with BRC calculations with the same prompt energy cuts (dotted line). The agreement between the experimental points and the BRC evaluation is good, better than 3%. Theoretical values are almost all higher than the experimental ones. This is related to the fact that the high-energy part of the experimental PFNS is below the evaluated PFNS.

To obtain an estimate of the prompt neutron mean energy without energy cut (total mean energy), we fitted

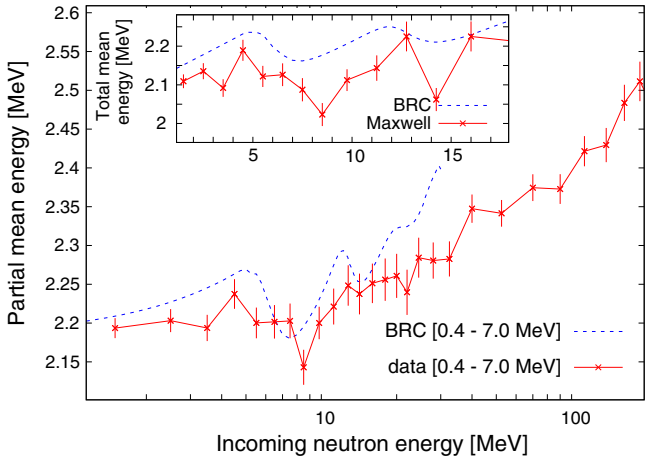

FIG. 8. (Color online) Evolution of the PFN mean energy with the incident neutron energy. (Dotted line) BRC calculation. (Crosses) Experimental results. (Main frame) Experimental and theoretical results are both calculated within a 400 keV to 7 MeV prompt energy cut. (Inset) Total mean energy extracted from a Maxwellian distribution and compared to BRC calculation without energy cut.

each spectrum with a Maxwellian distribution, which as a first approximation reproduces well the shape of the PFNS:

$$N(E) = \frac{2A\sqrt{E}}{\sqrt{\pi T_m^3}} \exp\left(-\frac{E}{T_m}\right). \quad (1)$$

T_m here is not the real temperature of the nucleus, but the free parameter of the distribution, proportional to the total mean energy:

$$\langle E_M \rangle = \tfrac{3}{2} T_m. \quad (2)$$

Results are presented in Table II and in the inset of the Fig. 8. We note that the statistical fluctuations are too important, mainly for the high-energy spectra, to get the fitting procedure to converge using a Watt distribution (describing the shape of the PFNS in the laboratory). However, for the cases where the convergence is reached, it gives results fully consistent with the ones obtained using a Maxwellian distribution.

TABLE II. Total mean energy extracted from fits of the PFNS by a Maxwellian distribution for different ranges in incident neutron energy.

Incident energy (MeV)	$\langle E_M \rangle$ (MeV)	Incident energy (MeV)	$\langle E_M \rangle$ (MeV)
1–5	2.132 ± 0.013	17–19	2.214 ± 0.041
1–2	2.110 ± 0.018	19–21	2.185 ± 0.041
2–3	2.135 ± 0.021	21–23	2.228 ± 0.041
3–4	2.092 ± 0.023	23–26	2.270 ± 0.039
4–5	2.189 ± 0.028	26–30	2.272 ± 0.037
5–6	2.122 ± 0.028	30–35	2.268 ± 0.035
6–7	2.126 ± 0.030	35–45	2.330 ± 0.029
7–8	2.088 ± 0.031	45–60	2.354 ± 0.027
8–9	2.023 ± 0.030	60–80	2.411 ± 0.028
9–10.5	2.112 ± 0.028	80–100	2.424 ± 0.031
10.5–12	2.143 ± 0.033	100–125	2.486 ± 0.032
12–13.5	2.225 ± 0.038	125–150	2.496 ± 0.035
13.5–15	2.062 ± 0.030	150–175	2.609 ± 0.040
15–17	2.2225 ± 0.039	175–200	2.636 ± 0.043

V. DISCUSSION

A. Sources of prompt fission neutrons

Prompt neutrons are emitted from different sources. At low excitation energy, they are thought to be mostly evaporated by the fully accelerated fission fragments, and depending on the incident neutron energy, they can also be emitted before fission.

First of all, when the neutron energy is higher than the fission barrier, the compound nucleus gets enough excitation energy to evaporate one neutron and a competition starts between the first chance fission (n,f) and the second chance fission (n,nf) channels. With FIGARO, we measure all neutrons emitted in coincidence with fission: Prompt fission neutrons evaporated by the fission fragments of the compound nuclei ^{239,240}Pu, and neutrons evaporated by the compound nucleus ^{240}Pu, when a second chance fission occurs. Then, with increasing incident neutron energy, fission channels of higher order open up successively.

Secondly, at higher neutron energy (already at 14 MeV), the pre-equilibrium contribution starts to increase and becomes important, compared to the evaporation contributions originating from the compound nucleus and fragments. Those pre-equilibrium neutrons are mainly emitted at forward angles with higher kinetic energies, whereas the neutron detection system covers side angles and is most efficient from 400 keV to 7 MeV. The FIGARO setup is therefore mainly sensitive to the evaporation contributions, which are close to isotropic and follow (to first order) a Maxwellian distribution. The measurement essentially does not include the pre-equilibrium component. In the case of ^{235,238}U a Monte Carlo calculation estimated the missing fraction of neutrons in the FIGARO data because of the pre-equilibrium process [9,18,19]. While at 50 MeV the missing part of the pre-equilibrium neutrons represents 1.5% of the total number of fission neutrons, it increases up to ∼10% at 200 MeV, which in this last case represents 75% of the total mean energy. As a consequence, at high incident neutron energy, the mean energy measured by FIGARO and given in Tables II and III, is an underestimation of the actual total mean energy value.

B. Trend of the compound nucleus temperature

In the present measurement, the general trend of the mean energy is an increase of about 15% over the incident neutron energy range from 1 to 200 MeV, as measured with detectors at 45°–135° with respect to the incoming neutrons (see Fig. 8). On average, the temperature of the compound nucleus is increasing with the incident neutron energy, so the prompt neutrons will globally be emitted with higher kinetic energy for higher incident neutron energies. This is confirmed by the spectral shape of the ratios data (cf. Fig. 7).

TABLE III. Total mean energy extracted from the fit of the PFNS by a Maxwellian distribution for different ranges in incident neutron energy.

Incident energy (MeV)	$\langle E_M \rangle$ (MeV)	Incident energy (MeV)	$\langle E_M \rangle$ (MeV)
1–3	2.124 ± 0.015	13–15	2.158 ± 0.034
3–5	2.138 ± 0.019	15–18	2.168 ± 0.034
5–7	2.124 ± 0.022	18–21	2.178 ± 0.034
7–9	2.059 ± 0.023	21–24	2.303 ± 0.038
9–11	2.108 ± 0.026	24–28	2.303 ± 0.035
11–13	2.217 ± 0.032	28–32	2.331 ± 0.040

However, the rise of the mean energy, thus the rise of the temperature, seems to start only around 12 MeV incident neutron energy (corresponding to 18 MeV excitation energy). Below this value and except for the dip at 7 MeV, the mean energy of the prompt neutrons seems somewhat flat, taking into account the statistical fluctuations. The same observation can be made for the previously studied reactions ^{238}U(n,f) and ^{237}Np(n,f) [9–11]. In Fig. 9 and in Table III the mean energy is recalculated on larger incident neutron energy ranges to reduce the statistic uncertainties. At least, up to the second chance (7 MeV incident neutron energy and 12 MeV of excitation energy), the mean energy of the prompt neutrons is constant (around 2.13 MeV; see Tables II and III). Therefore fission fragments seem to be produced at constant temperature, which is supporting the description of the compound nucleus also by a constant temperature level density and not by a Fermi gas level density. In Ref. [20] this model was successfully used to fit experimental level densities for nuclei from F to Cf, at excitation energies up to the neutron binding energy. Our data tend to show that this hypothesis is also valid at higher excitation energy. This agrees with the energy sorting hypothesis detailed in [5–7], where the level densities of the compound nuclei and fission fragments are described with a constant temperature level density, in which the temperature T depends on mass as $A^{-2/3}$. This dependency implies that the fission fragments mass distribution should be somewhat stable on this excitation energy range. This description disagrees with evaluations which use an increasing temperature model already at low excitation energy and describes both fragments with the adiabatic hypothesis leading to the same temperature, whereas in the constant temperature level density the heavy fragment has a lower temperature than the light fragment.

At low incident neutron energy, our experimental mean energy data (stable at least up to 7 MeV incident neutron energy) show indications of this disagreement with the BRC, JEFF 3.1, and ENDF/BVII.1 calculations. However, the statistical fluctuations on the ratio data are too important to confirm this disagreement.

Finally at higher incident neutron energy, PFNS descriptions given by all evaluations reproduce very well the experimental observables within the statistical uncertainties.

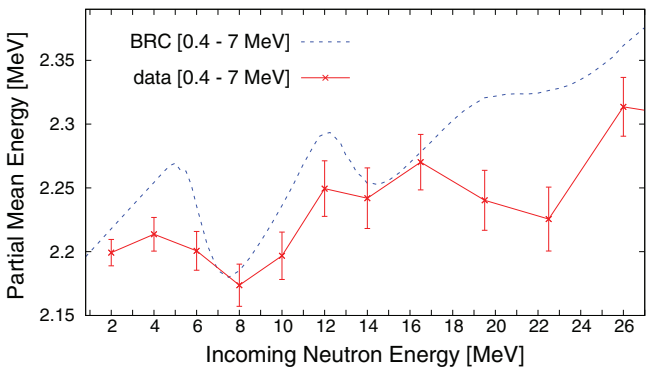

FIG. 9. (Color online) Prompt fission neutron mean energy (calculated within a 400 keV to 7 MeV prompt energy cut) as a function of the neutron beam energy, with larger incident neutron energy ranges than in Fig. 8. (Dotted line) BRC calculation. (Crosses) Experimental results.

C. Second chance fission

Figures 8 and 9 show that the measured mean energy significantly drops around 7 MeV, which is well reproduced by the BRC calculations. Figure 10 presents both calculated evaporation contributions in the laboratory frame (dotted line for the compound nuclei and upper dashed line for the fission fragments). This figure illustrates that the dip in the total mean energy appears when the second chance fission channel (n,nf) opens up. Its depth reflects the contribution of the pre-fission neutrons, because they are evaporated with less kinetic energy, mainly for two reasons: The compound nucleus has a lower temperature than the fission fragments and, contrary to the neutrons evaporated by the fission fragments, the ones evaporated by the compound nucleus are emitted in the laboratory frame and do not benefit from the fragment recoil velocity. BRC calculations quantify this last effect for the fission fragments case: Comparison between the

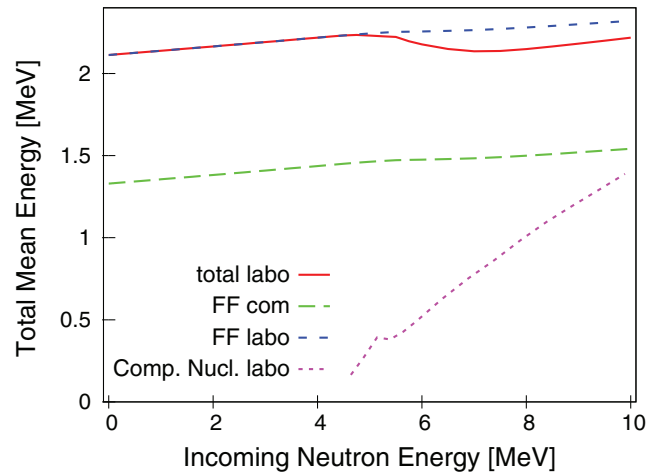

FIG. 10. (Color online) BRC calculation, without energy cut. (Dotted line) Mean energy of the neutrons evaporated by the compound nuclei before fission. (Dashed lines) Mean energy of the neutrons evaporated by the fully accelerated fission fragments in the laboratory frame (short dashed line above 2 MeV) and in the center of mass frame (long dashed line around 1.5 MeV). (Solid line) Total mean energy in the laboratory frame.

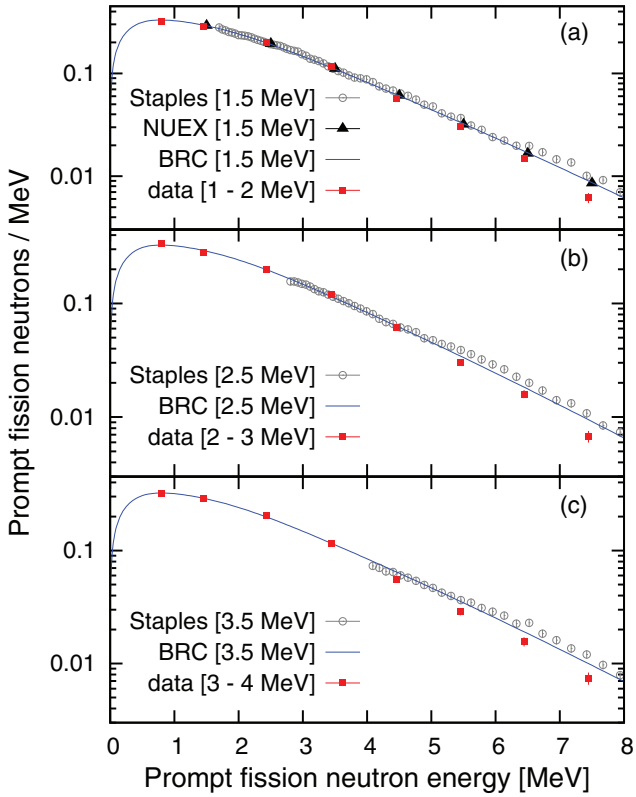

FIG. 11. (Color online) Comparison of PFNS (in logarithmic scale and at incoming neutron energy indicated into square brackets) between our data (solid squares), and BRC (solid line), data from Staples (open circles, [21]), and Lestone (NUEX, solid triangles, [22]).

two dashed lines in Fig. 10 shows that the emitter velocity contributes almost 1 MeV to the kinetic energy measured in the laboratory reference. Just at the opening of the second chance fission, the very first pre-fission neutrons emitted in coincidence with fission are evaporated with very low energy. The corresponding spectrum in the laboratory frame should present two well-marked contributions: evaporation by the fission fragments and, with a lower mean energy making the mean energy decrease, evaporation by the compound nucleus.

Finally, second and third small dips in the mean energy (Figs. 8 and 9) are visible around 14 and 20 MeV. Respectively, they are indications for the openings of the fission channel of third and fourth chance.

D. High-energy part of the PFNS

In Figs. 5 and 11 the logarithmic scale of the PFNS highlights discrepancies on the high-energy part of the spectra between our data and BRC (as shown in Fig. 6, for these energies, BRC results are close to the ones of JEFF 3.1 and ENDF/BVII.1) and previous measurements [21,22]. These last two measurements are different from the FIGARO data. In the experiment described in [21], fissions were induced by monoenergetic neutron beams and the ^{239}Pu target was a passive sample. Therefore fissions were not detected to trigger the acquisition system. As a consequence the PFNS had a threshold equal to the neutron beam energy to reject the contribution of the elastic and inelastic neutron scattering reactions from the data. However, these data describe well the high-energy part of the spectrum. Reference [22] described results obtained from the analysis of an underground nuclear test. In this experiment the emission of light charged particles, following the interaction of the prompt fission neutrons with a CH_2 foil, produced a current collected by a Faraday cup. This leakage current was then converted to PFNS. This kind of experiment benefits from very high statistics.

In Fig. 11, a larger binning is adopted to reduce the statistical uncertainties (error bars are included in the points) and each point is located at the bin mean energy. Agreement is excellent up to 4 MeV. As previously mentioned, we cannot rely on the efficiency correction for the high-energy part of the spectra. However if an experimental bias is introduced, it should be the same for each bin of incoming neutron energy. And it is clearly shown that for 3.5 MeV incoming neutron energy [see Fig. 11(c)] the disagreement is stronger than for 1.5 MeV [see Fig. 11(a)] and 2.5 MeV [see Fig. 11(b)].

As mentioned in the introduction, new calculations [2,4] propose a softer shape than what is currently evaluated. As a consequence the temperature of the neutron energy distribution would be lower than what is taken into account in the model. Figures 5 and 11 show that our measurements follow this trend. This explains why the experimental mean energy is globally lower than the theoretical one as shown in Figs. 8 and 9.

VI. CONCLUSION

PFNS were measured with the FIGARO setup for incident neutron energies from 1 to 200 MeV. It has to be kept in mind that these measurements are not very sensitive to the pre-equilibrium component because of the emission angles that were sampled. Therefore for incident neutrons of high energy, our data measure mainly the neutrons evaporated by the compound nuclei and the fission fragments.

The mean energy of the PFNS was measured with a statistical uncertainty better than 2%. Such a resolution provides a very good signature of the opening of second chance fission around 7 MeV. Moreover our data give also indications of the position of the opening of the $(n,2nf)$ and $(n,3nf)$ channels around 14 and 20 MeV.

In general, the data agree very well with the theoretical predictions based on the Los Alamos model. Below 4 MeV the agreement is excellent, also with previous data. However, the PFNS are softer than the predictions and previous data. We cannot conclude on this last point, because above 5 MeV (i) the data suffer from a lack of statistics and (ii) the efficiency correction is not reliable and might bias the data. Moreover, whereas the calculations predict a continuously increasing mean energy with the beam energy, experimental points seem somewhat constant within the error bars, at least up to the second chance and maybe up to 12 MeV incoming neutron energy. Such a behavior must definitely be confirmed by higher statistics experiments. This would sign a constant temperature of the compound nucleus for low and moderate excitation energies.

PFNS should continue to be explored experimentally, possibly with new detection methods to reduce background and increase the statistics. Such data would be able to discriminate between the different theoretical approaches. This would require new data for several neutron beam energies, with a higher precision especially for the description of low and high energy parts of the PFNS.

ACKNOWLEDGMENTS

This work was performed under the auspices of a cooperation agreement between CEA/DAM and DOE/NNSA on fundamental sciences and benefited from the use of the LANSCE accelerator facility, supported under DOE Contract No. DE-AC52-06NA25396.

[1] M. B. Chadwick *et al.*, Nucl. Data Sheets **112**, 2887 (2011).
[2] V. M. Maslov *et al.*, At. Energ. **108**, 432 (2010).
[3] P. Talou, B. Becker, T. Kawano, M. B. Chadwick, and Y. Danon, Phys. Rev. C **83**, 064612 (2011).
[4] B. Becker, P. Talou, T. Kawano, Y. Danon, and I. Stetcu, Phys. Rev. C **87**, 014617 (2013).
[5] K.-H. Schmidt and B. Jurado, Phys. Rev. Lett. **104**, 212501 (2010).
[6] K.-H. Schmidt and B. Jurado, Phys. Rev. C **83**, 014607 (2011).
[7] K.-H. Schmidt and B. Jurado, Phys. Rev. C **83**, 061601(R) (2011).
[8] D. G. Madland and J. R. Nix, Nucl. Sci. Eng. **81**, 213 (1982).
[9] T. Ethvignot *et al.*, Phys. Rev. Lett. **94**, 052701 (2005).
[10] T. Ethvignot *et al.*, Phys. Lett. B **575**, 221 (2003).
[11] J. Taieb *et al.*, in *Proceedings of International Conference in Nuclear Data for Science and Technology, Nice, France*, edited by O. Bersillon, F. Gunsing, E. Bauge, R. Jacqmin, and S. Leray (EDP Sciences, Les Ulis, 2007), p. 429.
[12] S. Noda *et al.*, Phys. Rev. C **83**, 034604 (2011).
[13] P. W. Lisowski *et al.*, Nucl. Instrum. Methods A **562**, 910 (2006).
[14] D. Rochman *et al.*, Nucl. Instrum. Methods A **523**, 102 (2004).
[15] W. Mannhart, in *Proceedings of IAEA Advisory Group Meeting Properties of Neutron Sources, TECDOC-410* (IAEA, Vienna, 1987), p. 158.
[16] A. Sardet *et al.*, Nucl. Instrum. Methods A (to be published).
[17] A. Tudora, G. Vladuca, and B. Morillon, Nucl. Phys. A **740**, 33 (2004).
[18] N. V. Kornilov and F.-J. Hambsch, Phys. Rev. Lett. **101**, 039201 (2008).
[19] T. Ethvignot *et al.*, Phys. Rev. Lett. **101**, 039202 (2008).
[20] T. von Egidy and D. Bucurescu, Phys. Rev. C **72**, 044311 (2005).
[21] P. Staples *et al.*, Nucl. Phys. A **591**, 41 (1995).
[22] J. P. Lestone and E. F. Shores, Los Alamos Report LA-UR-13-21239 (Los Alamos National Laboratory, Los Alamos, 2013).